JST: Engineering and Technology for Sustainable Development
Volume 34, Issue 1, March 2024, 035-042

Initial Research on the 1%CuO – 6CeO_2 – 4ZrO_2 Catalysts by TPR-H_2 for the Carbon Monoxide Preferential Oxidation (CO-PROX Reaction)

Ta Dinh Quang[1], Vuong Thanh Huyen[2], Le Minh Thang[1*]
[1]School of Chemistry and Life Sciences, Hanoi University of Science and Technology, Hanoi, Vietnam
[2] Leibniz Institute for Catalysts.e.V., Rostock, Germany
[*]Corresponding author email: thang.leminh@hust.edu.vn

Abstract

The 1wt%CuO – 6CeO_2 – 4ZrO_2 catalysts were synthesized by sol-gel method with two different procedures: (i) impregnating CuO on CeO_2-ZrO_2 support (CuO/CeO_2-ZrO_2), (ii) sol-gel of the Cu, Ce and Zr precursor together (CuO-CeO_2-ZrO_2). These catalysts were applied for the preferential oxidation of carbon monoxide (CO-PROX) to remove a small quantity of CO in an H_2-rich stream (the new research direction in Viet Nam), fueling the proton exchange membrane fuel cell (PEMFC) energy system. The findings of the TPR-H_2 experiment indicated that the catalyst produced through the first method exhibited an α reduction peak at 174 °C, which shows the effective dispersion of copper species. In combination with EPR results, the author anticipates a significant dispersion arising from isolated copper, which is recognized as a pivotal site in the CO-PROX reaction per numerous reputable studies. The catalyst synthesized by the second method did not provide a clear indication of the oxidation behavior of Cu-species. Therefore, it can be inferred that this catalyst is inappropriate for the low-temperature CO-PROX reaction.

Keywords: CuO-CeO_2-ZrO_2, TPR-H_2, CO-PROX reaction, PEMFC.

1. Introduction

Hydrogen-rich stream as fuel for the proton exchange membrane fuel cell (PEMFC) provides an alternative to fossil fuels in a world threatened by global warming and climate change. This is a powerful transformation technology in the transportation industry for reducing CO_2 emissions. The PEMFC can operate at low temperatures (60-150 °C), does not release CO_2, has a theoretical efficiency of up to 83%, and meets green energy standards [1]. The primary techniques for obtaining the H_2 supply for PEMFC are steam reforming and water gas shift reaction (WGS). The CO level of the H_2-rich gas stream at the end of the process is approximately 0.5-2%, which might induce poisoning of the Pt anode in the PEMFC [2]. This leads to a reduction in the performance of the PEMFC by up to 50% [3]. CO preferential oxidation (CO-PROX) appears to be the most straightforward and cost-effective way of reducing CO concentration to ppm levels [4]. The CO-PROX has undergone significant study and testing, and it is well suited for usage in small stationary equipment, such as electric vehicles powered by PEMFC batteries [5].

Three main groups of catalysts were studied for the CO-PROX reaction: (i) noble metal catalysts, (ii) gold-based catalysts, and (iii) transition metal catalysts. The platinum groups showed excellent conversion ability and selectivity. However, industrial application, mainly small-scale installation into PEMFC-powered vehicles, is impossible and un-economical because of their scarcity and high cost [6]. Gold-based catalysts also have potential in the CO-PROX reaction. However, rising the temperature leads to decreased selectivity due to the competitive oxidation of H_2, resulting in a loss of H_2 in the feedstock [7]. Therefore, gold-based catalysts are unsuitable for industrial-scale applications. With low costs and high performance, transition metal catalysts could replace noble metals and gold-based catalysts. Because of its unique properties for the CO-PROX, the CuO-CeO_2 binary catalyst system has been extensively documented in the literature [8]. Also, reaction efficiency is improving due to the Cu-Ce interactions resulting from the unstable exchange of ion pair: $Cu^{2+} + Ce^{3+} \Leftrightarrow Cu^{+} + Ce^{4+}$. The performance of CuO-CeO_2 in the preferential oxidation reaction has been demonstrated relating to finely dispersed Cu-species on the ceria surface. This phenomenon promotes oxygen vacancy generation at the CuO-CeO_2 boundary, which in turn enhances the reduction capacity of CuO [9].

Zirconium dioxide (ZrO_2) is a highly surface acid that maintains stability under elevated temperatures. Adding ZrO_2 enhances the thermal resistance of CeO_2 and the stability of the resulting oxide mixture [10].

ISSN 2734-9381
https://doi.org/10.51316/jst.172.etsd.2024.34.1.5
Received: 21 Dec 2023; revised: 6 Feb 2024;
accepted: 6 Feb 2024

Furthermore, incorporating ZrO_2 can result in the formation of a CeO_2-ZrO_2 solid solution, thereby increasing the oxygen storage, redox capacity, and retarding crystal-line growth of CeO_2 [11]. Ratnasamy *et al.* synthesized a catalyst consisting of 5 wt% CuO support on $6CeO_2$-$4ZrO_2$ (molar ratio). The resulting catalyst exhibited comparable activity to a catalyst composed of CuO-CeO_2 while demonstrating sustained stability for 18 hours. A noteworthy aspect is that the selectivity of the CuO/CeO_2-ZrO_2 catalyst is superior to the CuO-CeO_2, even under realistic conditions involving feedstock containing H_2O and CO_2 [12]. Beyond that, in a study conducted by Martínez *et al*., it was demonstrated that catalysts with a 1 wt% CuO content exhibited better activity compared to catalysts with 2% and 4% loading. Surprisingly, the conversion rates do not show a significant exponential difference based on the mass ratio of Cu, and the variation does not appear to be too substantial. In addition, the study revealed that the dispersion of CuO in the catalysts plays an important role in the CO-PROX reaction [13].

Despite yielding favorable outcomes, there is a scarcity of publications about the CuO-CeO_2-ZrO_2 catalysts in the context of the CO-PROX reaction. Thus, the authors aimed to create a catalyst with 1% CuO on CeO_2-ZrO_2 support in order to explore the potential for optimizing the CuO load. Specifically, we aimed to determine if achieving high conversion efficiency with a lower CuO loading is feasible. Therefore, we have prepared 1wt%CuO-$6CeO_2$-$4ZrO_2$ with two different procedures using the sol-gel method to apply for the CO-PROX reaction. Subsequently, the samples underwent physiochemical characterization using BET, EDS, and ICP techniques. The redox behavior of catalysts was conducted using TPR-H_2, while EPR examined Cu-species in the catalyst. This preliminary characterization is expected to enable the derivation of conclusions regarding the ability of catalysts to oxidize CO in a hydrogen-rich stream environment, thereby paving the way for its potential application in the future for the CO-PROX reaction. Simultaneously, this allows for anticipating an appreciative catalytic synthesis approach for prospective investigations.

2. Experiment

2.1. Preparation 1%CuO/6CeO₂-4ZrO₂ (CuO Impregnated on CeO₂-ZrO₂ Support)

The CeO_2-ZrO_2 support with a Ce/Zr molar ratio of 6/4 was prepared by a sol-gel method. Firstly, 4.885 grams of $Ce(NO_3)_2.6H_2O$ were dissolved in 20 ml of H_2O, and 10 ml of NH_3 25% was added to this solution and stirred until homogeneous at 60 °C. Then, 2.417 grams of $ZrOCl_2.8H_2O$ and 4 grams of citric acid as a complexing agent were added to the Ce^{4+} solution. The resulting mixture was stirred at 60 °C for 1 hour. In the next step, acid nitric 0.1 M was added dropwise under continuous stirring to form a suspension by hydrolysis. Continue stirring until the combination had a yellow gel. To create an aerogel, the gel was eventually aged at supercritical conditions of 60 ml ethanol in an autoclave at a temperature of 245 °C for 12 hours. After filtration and washing with distilled water, the sample was dried at 120 °C for 12 hours, followed by calcination at 500 °C for 3 hours in static air to form CeO_2-ZrO_2 support. 1wt%CuO/$6CeO_2$-$4ZrO_2$ with 1wt% CuO loading were synthesized in the same way, but in the first step, the prepared CeO_2-ZrO_2 support was dissolved with 0.2218 grams of $Cu(NO_3)_2.3H_2O$, 4.0 grams of citric acid in 25 ml of ethanol at 60 °C for 6 hours. Then, nitric acid was added, and the hydrolysis in an autoclave, the filtration, drying, and calcination were performed under the same conditions as above. This sample is named Cat1.

2.2. Preparation 1%CuO-6CeO₂-4ZrO₂ (a homogeneous mixture of CuO - CeO₂-ZrO₂)

1wt%CuO-$6CeO_2$-$4ZrO_2$ (Ce and Zr molar ratio) was synthesized by the sol-gel method from a precursor solution. To begin with, 4.885 grams of $Ce(NO_3)_2.6H_2O$ was dissolved in 20 ml of distilled water, and 10 ml of NH_3 25% was added to this solution and stirred until homogeneous at 60 °C. Then, 2.417 grams of $ZrOCl_2.8H_2O$, 4.0 grams of acid citric, and 0.2218 grams of $Cu(NO_3)_2.3H_2O$ were added to the Ce^{4+} solution. The resulting mixture was stirred at 60 °C for 1 hour. The nitric acid 0.1 M was added dropwise under continuous stirring to form a suspension by hydrolysis. Continue stirring for 3 hours until the combination has a yellow gel. The gel was eventually aged at supercritical conditions of 60 ml Ethanol in an autoclave at 245 °C for 12 hours. Filter and wash with distilled water, then dry the obtained sample at 120 °C for 12 hours. Followed by calcination at 500 °C for 3 hours. This sample catalyst is named Cat2.

2.3. Catalysts Characterization

The specific area (S_{BET}) and average pore diameter (d_{pore}) were determined by conducting Nitrogen adsorption measurements on a Micromeritics ASAP 2010 instrument. Electron Paramagnetic Resonance (EPR) spectroscopy was performed using Bruker EMX-Micro. This study employed a microwave power of 6.3 mW, a modulation frequency of 100 kHz, an amplitude of 0.5 mT at room temperature, and a magnetic field of up to 5000G. The hydrogen temperature programmed reduction (TPR-H_2) profiles were obtained using an Autochem II 2920 instrument (Micromeritics, Norcross, USA). A quartz reactor with a U-shape configuration was utilized to load a sample weighing 100 mg. The reactor was heated at 10 °C/min in a He gas flow (50 mL/min). The temperature was raised to 300 °C and maintained for 1 hour to eliminate any adsorbed species in the sample.

Subsequently, the system was cooled to 50 °C, facilitated by a He gas flow. TPR-H_2 experiment was conducted using a 5%H_2/Ar gas mixture (30 mL/min). The temperature was increased from 25 °C to 900 °C at a heating rate of 10 °C/min. The measurement of H_2 consumption was continuously monitored utilizing a thermal conductivity detector. Element distribution mapping was examined using a JEOL JCM-7000 (Japan). EDS is equipped with an X-ray microscope analyzer spectrometer (Benchtop SEM). The elemental composition was analyzed using inductively coupled plasma optical emission spectroscopy (ICP-OES) with a 715-ES ICP spectrometer (Varian, Palo Alto, CA, USA). The sample was dissolved in a mixture of hydrofluoric acid and aquilegia at 200 °C and 60 bar.

3. Results and Discussion

3.1. Physical Adsorption Results

N_2 adsorption/desorption isotherms and average pore diameter distributions are displayed in Fig 1. Based on the 2015 IUPAC classification, it can be observed that all the catalysts exhibit type IV(a) isotherm, which is indicative of mesoporous materials. The presence of micropores is associated with a distinct mechanism involving forming multiple layers followed by capillary condensation. This process results in the observation of Type IV(a) or Type IV(b) isotherms, and Type IV(a) is characterized by the occurrence of capillary condensation within mesopores (>4nm) [14].

Cat1 showed a type H_2 hysteresis loop ($0.6<P/P_o<1$); this phenomenon arises when the distribution of pore cavity sizes is significantly broader than neck size. Cat2 represents a type H_3 hysteresis loop ($0.45<P/P_o<1$) associated with slit-like pores and plate-like particles [14].

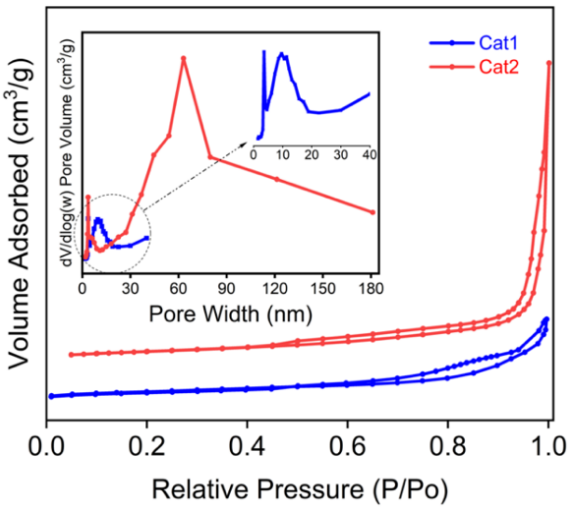

Fig. 1. N_2 adsorption/desorption isotherms and pore size distribution

Table 1. S_{BET} and average d_{pore} of two catalysts

Catalysts	S_{BET} (m^2/g)	Average d_{pore} (nm)
Cat1	43.33	10.01
Cat2	48.58	21.89

Table 1 shows the S_{BET} and d_{pore} of the two samples; the data reveals that the disparity in specific surface area between the two catalysts is negligible; however, the average pore size of Cat1 is approximately twice that of Cat2. In Fig. 1, the capillary distribution line shows that the Cat2 has an uneven distribution with a significant range from 0 to 180 nm. A prominent peak at 60nm suggests the prevalence of large capillary sizes (>50 nm). Although Cat2 also has a peak in the area below 10 nm, similar to Cat1, but it is insignificant because the number of large capillary sizes still accounts for the majority.

In the case of Cat1, the capillary pore size is smaller than 40 nm; this unequivocally suggests that Cat1 can be classified as a material possessing medium capillary characteristics. Therefore, it seems like that Cat1 has the potential to enhance the dispersion of the surface (because the pore size is smaller), consequently facilitating the promotion of active sites for the CO-PROX reaction.

3.2. The Composition of Catalysts

The elemental composition determined by Energy Dispersive Spectroscopy (EDS) and inductively coupled plasma optical emission spectroscopy (ICP-OES) are presented in Table 2.

The results showed that the Cat1 catalyst exhibits an elemental ratio that aligns more closely with the theoretical expectations than Cat2. Cat2 showed a substantial loss of CuO when the loading was merely 0.15%, whereas the hypothetical loading was 1%. As mentioned above, many investigations have demonstrated the importance of the synergistic interaction between CuO-CeO_2 in the context of the CO-PROX reaction. Consequently, utilizing a reduced quantity of Cu may exert a discernible influence on the overall catalytic efficacy.

Table 2. wt%CuO loading and Ce/Zr molar ratio determined by EDS and ICP

Catalysts	EDS		ICP	
	Ce/Zr atomic ratio	wt% CuO loading	Ce/Zr atomic ratio	wt% CuO loading
Cat1	1.56	1.24	1.40	1.22
Cat2	1.66	0.15	1.39	0.14

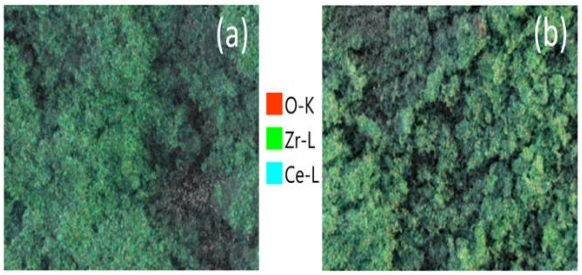

Fig. 2. EDS mapping (a) Cat1 and (b) Cat2

The elemental distribution mapping findings are visually depicted in Fig. 2. The observed distribution of Ce and Zr elements exhibits relatively uniformity. Nevertheless, with a low load of merely 1%, the presence of Cu was not discernible on the elemental distribution images obtained through EDS mapping. Therefore, the author can formulate an initial hypothesis suggesting that the Cu species in both Cat1 and Cat2 catalysts exhibit a high dispersion.

Due to the relatively low loading of Cu employed in this investigation, specifically 1 wt%, along with the EDS findings, which indicate that the Cu content in Cat2 is merely 0.15 wt%, this enormous loss of CuO prompts inquiries regarding the accuracy of the measurement. Henceforth, we employed the ICP technique to precisely ascertain the Cu content in both catalysts. The results presented in Table 2 confirmed that the Cu load in Cat2 was only 0.14%, pointing to a loss of material during the synthesis process of Cat2. In the second method, as the simultaneous sol-gel of Cu-Ce-Zr precursor solution, it seems like that Cu was lost significantly. This contrasts with the first method, where CeO_2-ZrO_2 is synthesized separately, and then copper precursor is added later. The loss of Cu^{2+} and other ions in the filtrate may occur during the filtration after the aging step in the autoclave. The loss of ions depends on the ability to precipitate each ion. The results showed that Cu^{2+} may be lost easiest in the filtrate in the second synthesis method, i.e., Cu^{2+} is the most difficult to precipitate from a precursor solution containing Cu, Ce, and Zr ions. However, in the first synthesis method, CeO_2-ZrO_2 have been formed previously, and in the slurry of Cu^{2+} solution with CeO_2-ZrO_2 powder, Cu^{2+} may be retained better on CeO_2-ZrO_2 support's structure. During the aging in the autoclave at 245°C, Cu^{2+} may be replaced partly for Ce or Zr ions in the CeO_2-ZrO_2 structure. Therefore, it was more hardly lost in the filtrate than occurred for the second synthesis method. The loss of Ce ion compared to Zr ion was also observed from ICP results as the Ce/Zr molar ratio is a bit lower than the theoretical value (Ce/Zr=1.5). However, this loss is not significant and almost the same in both synthesis methods, suggesting that Ce and Zr ions are easier to precipitate than Cu ion and the Zr precipitate, then Ce precipitate may be formed firstly during the aging step in the autoclave, before the precipitate of the Cu ion.

Consequently, Cu ion was lost significantly in the filtrate of the second synthesis method. XRD patterns of the catalysts showed that both catalysts are mixtures of CeO_2 and ZrO_2. The peaks belonging to CuO were hard to be seen in Cat1 due to the low loading and were not observed in Cat2 due to the lost of Cu^{2+}, as explained above.

3.3. EPR Spectra

Electromagnetic resonance spectroscopy (EPR) is commonly utilized to investigate unpaired electron compounds. Since Cu^{2+} has an outermost electron shell of $3d^9$, this approach is compassionate for identifying Cu^{2+} species in the catalyst. Fig. 3 shows the EPR spectra of both catalysts.

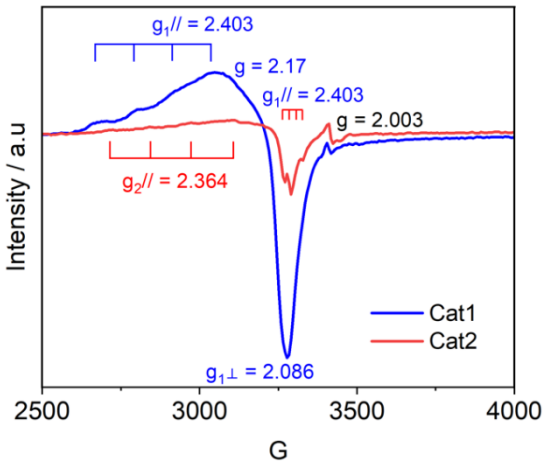

Fig. 3. EPR spectra of Cat1 and Cat2

While the EDS-mapping images did not exhibit visible traces of Cu, it is intriguing that the presence of Cu^{2+} ions was confirmed through EPR analysis. Furthermore, the axial signal depicted in Fig 3 showed that the amount of Cu^{2+} ions in Cat1 surpasses Cat2. These findings align with the elemental composition data presented in Table 2.

The two samples demonstrate signals with $g=2.003$, which can be attributed to electrons trapped in oxygen vacancies adjacent to Ce^{3+} (Ce^{3+}-O-□) or the defect Ce^{3+}-O-Ce^{4+}. Beside this signal, both Cat1 and Cat2 show signal of isolated Cu^{2+} species at ($g_{\perp}=2,086$, $g_{//}=2.403$, $A_{\perp}=82MHz$, $A_{//}=267MHz$) and ($g_{\perp}=2.082$, $g_{//}=2.364$, $A_{\perp}=63MHz$, $A_{//}=291MHz$), respectively. The slight difference in the parameters of their signals indicates the coupling of the single electron spin (d^9, $S=1/2$) with the nuclear spin of Cu ($I=3/2$) in two different local environments [15].

Moreover, the broad signal at $g=2.17$ in the Cat1 (which makes ultrafine separation impossible) is explained by the polarity of the dielectric expansion effect generated by interactions between paramagnetic Cu^{2+} ions. This indicates that the ions are in the Cu^{2+} synthetic phase of an oxide. Furthermore, since antiferromagnetic couplings between Cu^{2+} and CuO in

well-crystallized CuO phases result in EPR-silent species, the broad signal region is assumed to be composed of tiny clusters of copper oxide [16].

3.4. The Reducibility of the Catalysts

The catalyst underwent analysis using TPR-H_2 to ascertain reduction potential and surface oxidation patterns. According to research [17], it has been observed that pure CeO_2 typically displays two discernible peaks related to reduction from Ce^{4+} to Ce^{3+} at approximately 500 °C corresponding to reduction moderate in the surface layer of ceria atoms transitioning and the substantial reduction of bulk ceria oxide crystals at about 750 °C. Since the high temperature requirements, achieving a complete reduction of CeO_2 to Ce_2O_3 is not feasible. The shifting of reduction peaks towards lower temperatures, as depicted in Fig. 4, suggests that adding Cu and Zr enhances the initial redox capacity of CeO_2. The detection of the typical reduction peak of ZrO_2 is impeded due to the fact that this oxide cannot be reduced at temperatures below 1200°C. Cat1 and Cat2 exhibit a substantial reduction of bulk ceria oxide crystals from the Ce^{4+} to Ce^{3+} at around 750 °C. The reduction peaks observed in the 170-265 °C can be attributed to the reduction of Cu^{2+} to Cu^0 in the Cat1 [18].

Within the temperature around 450 °C assigned for the reduction of surface CeO_2 to Ce_2O_3, Cat1 exhibits a relatively feeble peak, whereas Cat2 manifests an exceedingly distinct peak. According to data presented in Table 3, it is evident that the disparity in H_2 consumption capacity between the two catalysts is negligible.

Table 3. H_2 consumption of catalysts

Catalysts	H_2 quantity (mmol/g)
Cat1	2.02
Cat2	2.10

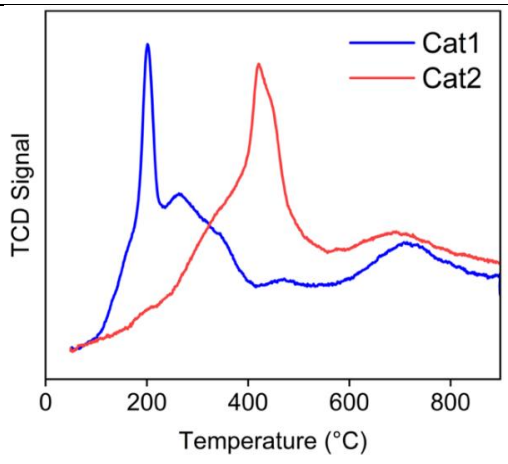

Fig. 4. TPR-H_2 profile of Cat1 and Cat2

Moreover, the temperature range at which the peak of Cat1 occurs is comparatively lower than that of Cat2. The primary focus of investigations of the CO-PROX reaction is to analyze the catalyst performance within the operational temperature range of the PEMFC (60-150 °C). Thus, based on the observed redox behavior, it can be inferred that Cat1 exhibits more outstanding suitability for the CO-PROX reaction than Cat2.

According to previous research, particularly the extensive investigation conducted by Arias *et al.* [19] utilizing advanced *in-situ* spectroscopy concluded that Cu^+ species serve as oxygen sites. CO conversion is active in the CuO-CeO_2 catalyst, followed by formation and stabilization promoted through $Cu^{2+} + Ce^{3+} \Leftrightarrow Cu^+ + Ce^{4+}$ interactions. Hence, it can be reaffirmed that Cat1, which exhibits low-temperature reduction peaks associated with Cu, possesses greater potential for utilization in the CO-PROX reaction than Cat2. The mechanism is as follows [20]:

$$Cu^{2+} + CO + O^{2-} \Leftrightarrow 2Cu^{+} + CO_2$$

$$\text{and/or } Cu^{2+} + CO + O^{2-} \Leftrightarrow Cu^0 + CO_2 \quad (1)$$

$$2Cu^{+} + 2Ce^{4+} \Leftrightarrow 2Cu^{2+} + 2Ce^{3+}$$

$$\text{and/or } Cu^0 + 2Ce^{4+} \Leftrightarrow Cu^{2+} + 2Ce^{3+} \quad (2)$$

$$2Ce^{3+} + ½\ O_2 \Leftrightarrow 2Ce^{4+} + O^{2-} \quad (3)$$

In the first step, CO undergoes oxidation by accepting oxygen from copper ions (Cu^{2+}), resulting in the formation of CO_2. The reaction under consideration can generate both Cu^+ and Cu^0 species concurrently. In the second step, the Cu^+ and Cu^0 species undergo reoxidation by Ce^{4+} to yield Cu^{2+} and Ce^{3+} ions. In the third step of the process, the Ce^{3+} species undergoes reoxidation to Ce^{4+} through the interaction with the O_2 present in the feed. In this context, the redox pair Cu^{2+}/Cu^+ and Ce^{4+}/Ce^{3+} participate in the reaction to create a synergistic interaction. O_2 enters the CeO_2 lattice, then moves to the vicinity of the isolated Cu^{2+} atom, and then combines with CO to form CO_2.

Probably, the direct oxidation mechanism originating from Cu^{2+} must not be disregarded, wherein O_2 infiltrates a designated Cu site and is directly eliminated through a reaction with CO.

$$4Cu^{+} + O_2 \Leftrightarrow 4Cu^{2+} + O^{2-}$$

$$\text{and/or } 2Cu^0 + O_2 \Leftrightarrow 2Cu^{2+} + 2O^{2-} \quad (4)$$

To provide a more comprehensive elucidation, the author has undertaken a TPR-H_2 profile overlapping peaks analysis of the catalysts to understand better the Cu species actual function and significance in Fig. 5.

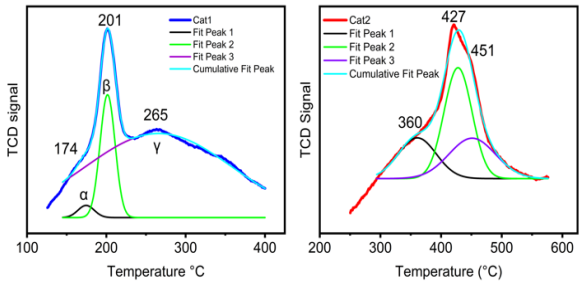

Fig. 5. The cumulative fitting peak of catalysts

Numerous authors have proposed, and a consensus among scholars has been reached that the observed peaks in TPR-H_2 reduction can be attributed to Cu species present on a support material closely associated with CeO_2. According to Avgouropoulos *et al.* [21], the presence of highly dispersed CuO in conjunction with CeO_2 and bulk CuO particles was found to be accountable for the occurrence of the lowest *(α)* and highest *(γ)* temperature peaks, respectively. Previous research has identified three prominent reduction peaks for Cu in the TPR-H_2 profile:

(i) A peak observed at approximately 125-150 °C suggests the existence of CuOx species that are evenly distributed on the supports [22].

(ii) The observed peak at about 200 °C can be attributed to the oxygen consumption in the Cu-[Ox]-Ce species, which indicates the extent of interaction within this structure [23].

(iii) The temperature range of 250-300 °C is associated with the peaks observed in the reduction of CuO by H_2, mainly when dealing with larger-sized particles [24].

Due to the difference in materials and synthesis procedures, we argue that the CuO reduction peaks in the TPR-H_2 profile of this study are determined as follows:

(i) The α peak is observed in Cat1, indicating a high dispersion of CuOx species.

(ii) The β peak in Cat1, indicating the occurrence of defects substituted within the ceria oxide lattice. The reduction process can be outlined as follows:

$$Ce^{4+}\text{-}O\text{-}Cu^{2+}\text{-}O\text{-}Ce^{4+} + 2H_2 \Leftrightarrow Cu^0 + 2Ce^{3+} + 2H_2O$$

(iii) The γ peaks are displayed of the reduction of CuO particles of larger size. This peak is observed on the right shoulder for Cat1 and the left shoulder for Cat2.

Based on (1) to (4), Cu^{2+} is the first factor involved in CO oxidation, regardless of whether the reaction proceeds through direct or indirect pathways. The TPR-H_2 findings indicate that the α and β peaks observed in the Cat1 are characteristic of Cu species that are highly dispersed; this aligns with the hypothesis derived from the EDS-mapping results. Moreover, the EPR findings provide compelling evidence supporting the existence of isolated Cu^{2+} sites in the Cat1. All of this confirms that the α and β peaks on the TPR-H_2 profile are a critical factor in the Carbon Monoxide Preferential Oxidation reaction. This means Cat1 is more suitable as a catalyst for the CO-PROX reaction than Cat2.

Cat1 showed the γ peak at 265 °C; it can be assigned with the reduction of large CuO clusters. Additionally, the broadening of the peak's foot on the higher temperature side, spanning from 265 to 400 °C, can be ascribed to the modest interaction between Cu and Ce, which interaction serves to lower the reduction temperature of the oxide in question. Indeed, the presence of CeO_2 support facilitates a decrease in the reduction temperature of copper oxide species [18]. Lou *et al.* [25] have substantiated the role of Ce in promoting the reduction of Cu species widely dispersed on the surface. However, the effectiveness of this reduction process is contingent upon the size of the CuO particles; specifically, smaller particles exhibit greater ease of reduction. Hence, the shoulder at 360°C of Cat2 could imply that the copper particles in this catalyst have a large size.

The peaks at 427 °C and 451 °C has been attributed to the reduction of Cu-[Ox]-Ce species and surface CeO_2, respectively, indicating that Cat2 exhibits a relatively feeble interaction CuO-CeO_2. The underlying cause can be attributed to the relatively low loading of CuO (0.15wt%) present on the CeO_2-ZrO_2 support. Beyond that, the CO-PROX reaction occurs at the interface between the metal ion and the support. The improved performance of copper catalysts supported by Ce can be attributed to sites formed at the periphery of nano copper grains [26]. Hence, the larger copper particles decrease the interfacial area, diminishing the strength of the metal support interaction.

Based on the observations above, it can be inferred that the peak γ exhibited by Cat1 and the reduction shoulder peak of Cat2 at 360 °C is the one factor that lowers the catalytic performance since the big CuO particles have been reported as less active for CO-PROX. There, it is imperative to note that Cat2 is unsuitable for engaging in low-temperature CO-PROX reactions.

Conclusion

The present investigation conducted a comprehensive analysis of the oxidation capacity utilizing the technique of TPR-H_2 of 1wt%CuO-6CeO_2-4ZrO_2 catalysts, which were synthesized through two distinct processes, impregnating CuO to CeO_2-ZrO_2 support and sol-gel synthesis from the

precursor solution of CuO-CeO_2-ZrO_2. The experimental findings indicate that Cat1 shows a propensity for oxidation at relatively low temperatures, aligning well with the operating window temperature in the CO-PROX reaction. Furthermore, it is evident that Cat1 exhibits a pronounced synergistic interplay between Cu and Ce in contrast to Cat2. Combining this with the EPR results, we can infer that the Cat1 exhibits a notable dispersion of isolated Cu^{2+} ions. Beyond that, EPR and TPR-H_2 results also confirmed the presence of CuO-cluster species in Cat1 and Cat2, which would reduce the catalytic activity in the CO-PROX reaction. This observation aligns perfectly with the mechanisms that have been previously established and validated. In brief, Cat1 will be chosen as the catalyst for the preferential oxidation of carbon monoxide in the hydrogen-rich gas stream part.

Acknowledgments

This research has been supported by the RoHan Project funded by the German Academic Exchange Service (DAAD, No. 57315854) and the Federal Ministry for Economic Cooperation and Development (BMZ) inside the framework "SDG Bilateral Graduate School programme."

References

[1] P. Sharma and O. P. Pandey, Chapter 1 - Proton exchange membrane fuel cells: fundamentals, advanced technologies, and practical applications, PEM Fuel Cells: Fundamentals, Advanced technologies, and Practical Application, G. Kaur, Ed. Elsevier, 2022, pp. 1–24. https://doi.org/10.1016/B978-0-12-823708-3.00006-7

[2] G. Xiang *et al*., Atomically dispersed Au catalysts for preferential oxidation of CO in H_2-rich stream, Appl. Catal. B Environ., vol. 296, p. 120385, 2021. https://doi.org/10.1016/j.apcatb.2021.120385

[3] Z. Boukha, J. R. González-Velasco, and M. A. Gutiérrez-Ortiz, Exceptional performance of gold supported on fluoridated hydroxyapatite catalysts in CO-cleanup of H_2-rich stream: High activity and resistance under PEMFC operation conditions, Appl. Catal. B Environ., vol. 292, p. 120142, 2021. https://doi.org/10.1016/j.apcatb.2021.120142

[4] V. Palma, C. Ruocco, M. Martino, E. Meloni, and A. Ricca, Catalysts for conversion of synthesis gas, in Bioenergy Systems for the Future, Elsevier, 2017, pp. 217–277. https://doi.org/10.1016/B978-0-08-101031-0.00007-7

[5] E. Poggio-Fraccari, A. Abele, N. Zitta, J. Francesconi, and F. Mariño, CO removal for hydrogen purification via Water Gas Shift and CO-PROX reactions with monolithic catalysts, Fuel, vol. 310, p. 122419, 2022. https://doi.org/10.1016/j.fuel.2021.122419

[6] Y. Chen, J. Lin, L. Li, X. Pan, X. Wang, and T. Zhang, Local structure of Pt species dictates remarkable performance on Pt/A_2O_3 for preferential oxidation of CO in H_2, Appl. Catal. B Environ., vol. 282, p. 119588, 2021 https://doi.org/10.1016/j.apcatb.2020.119588.

[7] L.-H. Chang, Y.-L. Yeh, and Y.-W. Chen, Preferential oxidation of CO in hydrogen stream over nano-gold catalysts prepared by photodeposition method, Int. J. Hydrogen Energy, vol. 33, no. 7, pp. 1965–1974, 2008. https://doi.org/10.1016/j.ijhydene.2008.01.014

[8] Q. Zou *et al*., Ceria-nano supported copper oxide catalysts for CO preferential oxidation: Importance of oxygen species and metal-support interaction, Appl. Surf. Sci., vol. 494, pp. 1166–1176, 2019. https://doi.org/10.1016/j.apsusc.2019.07.210

[9] A. Di Benedetto, G. Landi, and L. Lisi, Improved CO-PROX performance of CuO/CeO_2 catalysts by using nanometric ceria as support, Catalysts, vol. 8, no. 5, p. 209, 2018. https://doi.org/10.3390/catal8050209

[10] J. Kašpar, P. Fornasiero, and N. Hickey, Automotive catalytic converters: current status and some perspectives, Catal. today, vol. 77, no. 4, pp. 419–449, 2003. https://doi.org/10.1016/S0920-5861(02)00384-X

[11] H. Vidal *et al*., Redox behavior of CeO_2–ZrO_2 mixed oxides: I. Influence of redox treatments on high surface area catalysts, Appl. Catal. B Environ., vol. 27, no. 1, pp. 49–63, 2000. https://doi.org/10.1016/S0926-3373(00)00138-7

[12] P. Ratnasamy et al., Influence of the support on the preferential oxidation of CO in hydrogen-rich steam reformates over the CuO–CeO_2–ZrO_2 system, J. Catal., vol. 221, no. 2, pp. 455–465, 2004. https://doi.org/10.1016/j.jcat.2003.09.006

[13] Martínez-Munuera, J. C., Giménez-Mañogil, J., Yeste, M. P., Hungría, A. B., Cauqui, M. A., García-García, A., & Calvino, J. J. (2022). New findings regarding the role of copper entity particle size on the performance of Cu/ceria-based catalysts in the CO-PROX reaction. Applied Surface Science, 575, 151717. https://doi.org/10.1016/j.apsusc.2021.151717

[14] K. A. Cychosz, R. Guillet-Nicolas, J. García-Martínez, and M. Thommes, Recent advances in the textural characterization of hierarchically structured nanoporous materials, Chem. Soc. Rev., vol. 46, no. 2, pp. 389–414, 2017. https://doi.org/10.1039/C6CS00391E

[15] J. Mosrati et al., Tiny Species with Big Impact: High Activity of Cu Single Atoms on CeO_2-TiO_2 Deciphered by Operando Spectroscopy, ACS Catal., vol. 11, no. 17, pp. 10933–10949, 2021 https://doi.org/10.1021/acscatal.1c02349.

[16] J. Chen, Y. Zhan, J. Zhu, C. Chen, X. Lin, and Q. Zheng, The synergetic mechanism between copper species and ceria in NO abatement over Cu/CeO_2 catalysts, Appl. Catal. A Gen., vol. 377, no. 1–2, pp. 121–127, 2010. https://doi.org/10.1016/j.apcata.2010.01.027

[17] A. Pintar, J. Batista, and S. Hočevar, TPR, TPO, and TPD examinations of $Cu_{0.15}Ce_{0.85}O_2$ mixed oxides

prepared by co-precipitation, by the sol-gel peroxide route, and by citric acid-assisted synthesis, J. Colloid Interface Sci., vol. 285, no. 1, pp. 218–231, 2005, https://doi.org/10.1016/j.jcis.2004.11.049.

[18] G. Avgouropoulos, T. Ioannides, and H. Matralis, Influence of the preparation method on the performance of CuO–CeO_2 catalysts for the selective oxidation of CO, Appl. Catal. B Environ., vol. 56, no. 1–2, pp. 87–93, 2005. https://doi.org/10.1016/j.apcatb.2004.07.017

[19] A. Martínez-Arias et al., Characterization of active sites/entities and redox/catalytic correlations in copper-ceria-based catalysts for preferential oxidation of CO in H_2-rich streams, Catalysts, vol. 3, no. 2, pp. 378–400, 2013, https://doi.org/10.3390/catal3020378.

[20] Wang, Feng, *et al*., In situ EPR study of the redox properties of CuO–CeO_2 catalysts for preferential CO oxidation (PROX), ACS catalysis 6.6 (2016): 3520-3530. https://doi.org/10.1021/acscatal.6b00589

[21] G. Avgouropoulos and T. Ioannides, Effect of synthesis parameters on catalytic properties of CuO-CeO_2, Appl. Catal. B Environ., vol. 67, no. 1, pp. 1–11, 2006. https://doi.org/10.1016/j.apcatb.2006.04.005

[22] F. Wang *et al*., A Photoactivated Cu–CeO_2 Catalyst with Cu-[O]-Ce Active Species Designed through MOF Crystal Engineering, Angew. Chemie, vol. 132, no. 21, pp. 8280–8286, 2020. https://doi.org/10.1002/ange.201916049

[23] X. Gong *et al*., Boosting Cu-Ce interaction in Cu_xO/CeO_2 nanocube catalysts for enhanced catalytic performance of preferential oxidation of CO in H_2-rich gases, Mol. Catal., vol. 436, pp. 90–99, 2017. https://doi.org/10.1016/j.mcat.2017.04.013

[24] X. Guo and R. Zhou, Identification of the nano/microstructure of CeO_2 (rod) and the essential role of interfacial copper-ceria interaction in CuCe (rod) for selective oxidation of CO in H_2-rich streams, J. Power Sources, vol. 361, pp. 39–53, 2017. https://doi.org/10.1016/j.jpowsour.2017.06.064

[25] M.-F. Luo, Y.-J. Zhong, X. Yuan, and X.-M. Zheng, TPR and TPD studies of CuO-CeO_2 catalysts for low temperature CO oxidation, Appl. Catal. A Gen., vol. 162, no. 1–2, pp. 121–131, 1997. https://doi.org/10.1016/S0926-860X(97)00089-6

[26] A. Arango-Díaz et al., Comparative study of CuO supported on CeO_2, $Ce_{0.8}Zr_{0.2}O_2$ and $Ce_{0.8}Al_{0.2}O_2$ based catalysts in the CO-PROX reaction, Int. J. Hydrogen Energy, vol. 39, no. 8, pp. 4102–4108, 2014. https://doi.org/10.1016/j.ijhydene.2013.04.062